Lead-Free Halide Double Perovskites via Heterovalent Substitution of Noble Metals

George Volonakis,[†,¶] Marina R. Filip,[†,¶] Amir Abbas Haghighirad,[‡] Nobuya Sakai,[‡] Bernard Wenger,[‡] Henry J. Snaith,[*,‡] and Feliciano Giustino[*,†]

†Department of Materials, University of Oxford, Parks Road OX1 3PH, Oxford, UK

‡Department of Physics, University of Oxford, Clarendon Laboratory, Parks Road, Oxford OX1 3PU, UK

¶These authors contributed equally to this work

E-mail: feliciano.giustino@materials.ox.ac.uk; henry.snaith@physics.ox.ac.uk

Phone: (+44) 1865 612790 ; (+44) 01865 272380

1

Abstract

Lead-based halide perovskites are emerging as the most promising class of materials for next generation optoelectronics. However, despite the enormous success of lead-halide perovskite solar cells, the issues of stability and toxicity are yet to be resolved. Here we report on the computational design and the experimental synthesis of a new family of Pb-free inorganic halide double-perovskites based on bismuth or antimony and noble metals. Using first-principles calculations we show that this hitherto unknown family of perovskites exhibits very promising optoelectronic properties, such as tunable band gaps in the visible range and low carrier effective masses. Furthermore, we successfully synthesize the double perovskite $Cs_2BiAgCl_6$, perform structural refinement using single-crystal X-ray diffraction, and characterize its optical properties via optical absorption and photoluminescence measurements. This new perovskite belongs to the $Fm\bar{3}m$ space group, and consists of $BiCl_6$ and $AgCl_6$ octahedra alternating in a rock-salt face-centered cubic structure. From UV-Vis and PL measurements we obtain an indirect gap of 2.2 eV.

Perovskites are among the most fascinating crystals, and play important roles in a variety of applications, including ferroelectricity, piezoelectricity, high-T_c superconductivity, ferromagnetism, giant magnetoresistance, photocatalysis and photovoltaics.[1–8] The majority of perovskites are oxides and are very stable under ambient temperature and pressure conditions.[4,9] However, this stability is usually accompanied by very large band gaps, therefore most oxide perovskites are not suitable candidates for optoelectronic applications. The most noteworthy exceptions are the ferroelectric perovskite oxides related to $LiNbO_3$, $BaTiO_3$, $Pb(Zr, Ti)O_3$ and $BiFeO_3$, which are being actively investigated for photovoltaic applications, reaching power conversion efficiencies of up to 8%.[9] The past five years witnessed a revolution in optoelectronic research with the discovery of the organic-inorganic lead-halide perovskite family. These solution-processable perovskites are fast becoming the most promising materials for the next generation of solar cells, achieving efficiencies above 20%.[10–13] Despite this breakthrough, hybrid lead-halide perovskites are known to degrade due to moisture and heat,[14] upon prolonged exposure to light,[15] and are prone to ion or halide vacancy migration, leading to unstable operation of photovoltaic devices.[16,17] At the same time the presence of lead raises concerns about the potential environmental impact of these materials.[18,19] Given these limitations, identifying a stable, non-toxic halide perovskite optoelectronic material is one of the key challenges to be addressed in the area of perovskite optoelectronics.

The starting point of our search for a lead-free halide-perovskite is the prototypical inorganic compound $CsPbI_3$. $CsPbI_3$ is an ABX_3 perovskite where the heavy metal cations Pb^{2+} and the halide anions I^- occupy the B and X sites, respectively, while Cs^+ occupies the A site. The most obvious route to replacing Pb in this compound is via substitution of other group-14 elements such as Sn and Ge. However both elements tend to undergo oxidation, for example from Sn^{2+} to Sn^{4+}, leading to a rapid degradation of the corresponding halide perovskites.[20–23] More generally, it should also be possible to substitute lead by other divalent cations outside of group-14 elements. However, our previous high-throughput computational screening of potential candidates showed that the homovalent substitution

of lead in halide perovskites impacts negatively the optoelectronic properties by increasing band gaps and effective masses.[24]

Another possible avenue is to consider heterovalent substitution, that is the formation of a double perovskite structure with a basic formula unit $A_2B'B''X_6$.[4] This type of compounds are abundant in the case of oxides and are well known for their ferroelectric, ferromagnetic and multiferroic properties.[4] Additionally, double perovskites have been explored in order to tune the band gap of oxide perovskites.[25,26] On the other hand, halide double perovskites remain a much less explored class of materials. To date, the best known halide double perovskites are based on alkali and rare-earth metals, and are investigated for applications as scintillators in radiation detectors.[27]

In order to replace the divalent Pb cations and maintain the total charge neutrality, the B' and B'' sites have to be occupied by one monovalent and one trivalent cation. We search for our B'^{3+} metallic cations among the pnictogens, and consider Bi and Sb as the most suitable choices. Arsenic is less desirable owing to its toxicity. For the monovalent cations we choose the noble metals Cu, Ag and Au. From elementary considerations Cu, Ag, and Au appear very promising for optoelectronic applications. In fact, in their metallic form, the noble metals are the best known electrical conductors, owing to their filled d^{10} shell and the free-electron-like behaviour of the s^1 shell. In addition, in an octahedral environment, the ionic radii of Cu^+ (0.91 Å), Ag^+ (1.29 Å) and Au^+ (1.51 Å) are similar to those of Pb^{2+} (1.19 Å), Sb^{3+} (0.76 Å) and Bi^{3+} (1.03 Å).[28] We note that the cost of the precursors for the proposed Pb-alternatives (AgCl and CuCl) are similar to the case of lead, except for the case of gold (AuCl) which is considerably more expensive. Following this simple reasoning we investigate hypothetical halide double perovskites with the pairs B'/B'' where B' = Sb, Bi, and B'' = Cu, Ag, Au.

We investigate the electronic properties of these hypothetical compounds from first principles using density functional theory (DFT) in the local density approximation (LDA). We construct 'rock-salt' double perovskites, whereby B' and B'' alternate in every direction

(shown in Figure 1a). The rock-salt ordering is known to be the ground state for most oxide double perovskites,[4] therefore it can be expected to hold also in the present case. For each model structure we perform full structural optimization using DFT-LDA and calculate the electronic band gaps using the hybrid PBE0 functional as described in the Supporting Information.

In Figure 1b-c we show a comparative view of the band gaps calculated for the entire $Cs_2B'B''X_6$ family. We find that all band gaps are below 2.7 eV, spanning the visible and near infrared optical spectrum. The band gaps are indirect and increase as we move up the halogen or the pnictogen column in the periodic table, but do not follow a monotonic trend with respect to the size of the noble metal cation. This behaviour can be explained by the character of the electronic states at the band edges. Indeed, a shown in Figure S1 of the Supporting Information, the conduction band bottom and valence band top in each case are predominantly of pnictogen-p and halogen-p character, respectively. As we move up in the periodic table the energy of the halogen-p states decreases, thus lowering the energy of the valence band top. Similarly, the energy of the pnictogen-p states decreases when moving up in the periodic table, thus lowering the energy of the conduction band bottom. The electron and hole effective masses calculated at the band edges exhibit an anisotropic behaviour in most cases (see Table S1). Throughout the entire family of compounds the electron masses are more isotropic than the hole masses. For clarity, in Figure 1 we report the conductivity effective masses,[29] as defined in the Supporting Information. We note that all compounds exhibit small carrier effective masses between 0.1 and 0.4 m_e, very close to those calculated for $CH_3NH_3PbI_3$ within the same level of theory.[30]

The electronic band structures of these halide double perovskites (shown in Figure S2 and S3) exhibit several features of particular interest. In all cases, the valence band maximum (VBM) is at the X $(0,0,2\pi/a)$ point in the Brillouin zone. The conduction band minimum (CBM) is at Γ $(0,0,0)$ for $Cs_2BiAgCl_6$, $Cs_2BiCuCl_6$ and $Cs_2BiCuBr_6$, while for the other compounds the CBM is at the L $(\pi/a, \pi/a, \pi/a)$ point. In Figure S4, we show the band

structure of $Cs_2BiAgCl_6$ calculated in the conventional unit cell (which corresponds to four primitive cells and contains 8 octahedra in a cubic lattice). Here, as a result of Brillouin zone folding, the band gap of $Cs_2BiAgCl_6$ becomes direct at the Γ-point, although the direct transition is still forbidden by symmetry. This suggests an avenue for engineering a direct band gap in these compounds. In fact symmetry can be broken by inducing octahedral tilts, and this could be achieved by varying the steric size of the A-site cation (Cs).[31] For example, this effect could be realized by incorporating an organic cation, like methylammonium or formamidinium into the cuboctahedral cavity. In order to demonstrate this point, we report in Figure S5 the calculated band structure of the hypothetical orthorhombic compound $MA_2BiAgCl_6$ (MA $= CH_3NH_3$, methylammonium; the structure is constructed as described in the Supporting Information). Explicit calculations of the optical matrix elements indicate that the direct optical transition in the methylammonium-based compound is allowed, as expected.

Having established that the family of $A_2B'B''X_3$ halide double perovskites, based on $B' =$ Sb, Bi and $B'' =$ Cu, Ag, Au exhibits promising optoelectronic properties, we move to the synthesis and optical characterization of a representative member of this group of compounds. We adapt the synthesis process of $Cs_2BiNaCl_6$, reported in Ref.,[32] to allow for the incorporation of a noble metal. Of the three noble metals under consideration, Ag has an ionic radius which is closest to that of Na (1.02 Å vs 1.15 Å). For this reason we proceed to synthesize $Cs_2BiAgCl_6$ by conventional solid-state reaction as described in detail in the Supporting Information. In Figure 2a we show the X-ray Diffraction Pattern for a single crystal ($\sim 30\mu$m diameter). We observe sharp reflections for the crystallographic $0kl$, $h0l$ and $hk0$ planes. These reflections show characteristics of $m\bar{3}m$ symmetry that reveal systematic absences for (hkl; $h + k$, $k + l$, $h + l = 2n$) corresponding to the face-centered space groups $F432$, $F\bar{4}3m$ and $Fm\bar{3}m$. The latter was selected for structure refinement after confirmation that $Cs_2BiAgCl_6$ crystallizes in an FCC lattice. We find that there is no significant distortion of octahedral symmetry about the Bi^{3+}. The atomic positions from the

structural refinement are listed in Table S2 of the Supplementary Information. The X-ray diffraction patterns uniquely identify the $Fm\bar{3}m$ (no. 225) space group at room temperature, and the quantitative structural analysis gives a very good description of the data. In addition, our crystal structure refinement is consistent with the rock-salt configuration assumed by our atomistic model. The experimental and computationally predicted conventional lattice parameters are in very good agreement, 10.78 Å and 10.50 Å, respectively. From the optical absorption spectrum and Tauc plot (see Figure 2b) we can estimate an indirect optical band gap in the range of 2.3-2.5 eV. The indirect character of the band gap is consistent with the broad photoluminescence peak observed between 480 and 650 nm (1.9-2.6 eV) with the maximum at $\sim$575 nm (2.2 eV), red-shifted with respect to the optical absorption onset. In addition, the time-resolved photoluminescence decay shown in Figure 2c was fitted with a double exponential giving a fast component lifetime of 15 ns and a slow component lifetime of 100 ns.The as-made compound appears to be stable under ambient conditions for weeks after synthesis, with the bright yellow color persisting and no visible changes appearing in the powder X-ray diffraction patterns (see Figures S6 and S7).

In Figure 3 we show the electronic band structure of $Cs_2BiAgCl_6$ calculated for the as determined experimental crystal structure, with and without relativistic spin-orbit coupling effects. The features of the valence band edge are almost unchanged when the relativistic effects are included. This is consistent with the predominant Cl-p and Ag-d character of this band. By contrast, due to the large spin-orbit coupling, the conduction band edge splits in two bands, separated by more than 1.5 eV at the Γ point. This effect is not surprising, given that the character of the conduction band bottom is of primarily Bi-p character. For comparison, in the case of $Cs_2SbAgCl_6$ (see Figure S8) the spin-orbit splitting of the conduction band at the Γ point is of only 0.5 eV. The fundamental band gap is reduced by 0.4 eV upon inclusion of relativistic effects, and the shape of the conduction band is drastically different. Therefore, the inclusion of spin-orbit coupling is crucial for the correct description of the conduction band edge, bearing resemblance to the case of

$CH_3NH_3PbI_3$.[33,34] In the fully relativistic case we calculated an indirect band gap of 3.0 eV and lowest direct transition of 3.5 eV, in very close agreement with the results obtained for the model $Cs_2BiAgCl_6$ structure, discussed in Figure 1 [2.7 eV (indirect) and 3.3 eV (direct)]. The small difference in band gap of 0.2-0.3 eV is due to the small difference in volume between the experimental and predicted crystal structure. The calculated electronic band gaps are overestimated with respect to the measured optical band gap by approximately 0.5 eV. This quantitative discrepancy does not affect the qualitative physical trends of the band gaps discussed throughout this work, and can be associated to the approximations employed in our PBE0 calculations. A better agreement with experiment can be reached by fine-tuning the fraction of exact exchange, or by performing GW calculations.[35,36] The latter will be reported in a future work.

In summary, through a combined theoretical and experimental study, we have designed a new family of halide double-perovskite semiconductors based on pnictogens and noble metals. We used state-of-the-art first-principles calculations in order to explore trends in the electronic and optical properties in the entire family of double perovskites $A_2B'B''X_6$ with A = Cs, B' = Bi, Sb, B'' = Cu, Ag, Au, and X = Cl, Br, I. Our calculations revealed highly tunable carrier effective masses, and optical gaps across the visible range of the electromagnetic spectrum. We predicted all compounds to be indirect gap semiconductors, and proposed a simple strategy for turning them into direct-gap materials. We successfully synthesized $Cs_2BiAgCl_6$, and obtained a face-centered cubic double perovskite. Optical characterization confirmed our theoretical predictions, indicating an indirect gap semiconductor. Overall, the present work is the first detailed description of the structure and optoelectronic properties of the pnictogen-noble metal halide double perovskite family, and calls for many future experimental and theoretical studies in order to assess the full potential of these new materials. We expect that a complete mapping of the genome of halide double perovskites based on pnictogens and noble metals may unlock a world of new functional materials for photovoltaics, photocatalysis, photodetectors, light-emitting devices, piezoelectrics, and magnetoelectrics.

Supporting Information Available: Description of the computational setup, details on the materials synthesis and characterization and crystallographic data. All the electronic band structures for the pnictogen-noble metal double halide perovskites. Additional figures relevant to the discussions in this article. This material is available free of charge via the Internet http://pubs.acs.org.

Acknowledgement

Note added

During the preparation of this manuscript we became aware of the publication of two related papers: Ref.[38] (published February 7th, 2016) and Ref.[39] (published February 10th, 2016). The key difference between the present work and that of Ref.[38,39] is that we perform a computational screening of the entire family of pnictogen-noble metal double halide perovskites and perform experiments that confirm our predictions.

References

(1) Suntivich, J.; Gasteiger, H. A.; Yabuuchi, N.; Nakanashi, H.; Goodenough, J. B.; Shao-Horn, Y. *Nature Chemistry* **2011**, *3*, 546–550.

(2) Stranks, S.; Snaith, H. J. *Nature Nanotechology* **2015**, *10*, 391.

(3) Grätzel, M. *Nature Materials* **2014**, *13*, 838.

(4) Vasala, S.; Karppinen, M. *Prog. Solid State Chem.* **2015**, *4*, 1–36.

(5) Grinberg, L.; West, D. V.; Torres, M.; Gou, G.; Stein, D. M.; Wu, L.; Chen, G.; Gallo, E. M.; Akbashev, A. R.; Davies, P. K.; Spanier, J. E.; Rappe, A. M. *Nature* **2013**, *503*, 509–512.

(6) Ramesh, R.; Spaldin, N. A. *Nature Mater.* **2007**, *6*, 21–29.

(7) Rinjders, G.; Blank, D. H. A. *Nature* **2005**, *433*, 369–370.

(8) Ahn, C. H.; Rabe, K. M.; Triscone, J.-M. *Science* **2004**, *303*, 488–491.

(9) Fan, Z.; Sun, K.; Wang, J. *J. Mater. Chem. A* **2015**, *3*, 18809.

(10) Green, M.; Ho-Baillie, A.; Snaith, H. J. *Nature Photonics* **2014**, *8*, 506.

(11) Lee, M. M.; Teuscher, J.; Miyasaka, T.; Myrakami, T. N.; Snaith, H. J. *Science* **2012**, *338*, 643.

(12) Kim, H.-S.; Lee, C. R.; Im, J.-H.; Lee, K.-B.; Moehl, T.; Marchioro, A.; Moon, S.-J.; Humphry-Baker, R.; Yum, J.-H.; Moser, J. E.; Grätzel, M.; Park, N.-G. *Sci. Rep.* **2012**, *2*, 591.

(13) Best Research-Cell Efficiencies. `http://www.nrel.gov/ncpv/images/efficiency_chart.jpg`.

(14) Manser, J. S.; Saidaminov, M. I.; Christians, J. A.; Bakr, O. M.; Kamat, P. V. *Acc. Chem. Res.* **2016**, *49*, 330–338.

(15) Hoke, E. T.; Slotcavage, D. J.; Dohner, E. R.; Bowring, A. R.; Karunadasa, H. I.; McGehee, M. D. *Chem. Sci.* **2015**, *6*, 613–617.

(16) Eames, C.; Frost, J. M.; Barnes, P. R. F.; O'Regan, B. C.; Walsh, A.; Saiful Islam, M. *Nature Commun.* **2015**, *6*, 7497.

(17) Meloni, S.; Moehl, T.; Tress, W.; Grankvicius, M.; Saliba, M.; Hui, Y.; Gao, P.; Nazeeruddin, M. K.; Zakeeruddin, S. M.; Rothlisberger, U.; Grätzel, M. *Nature Commun.* **2016**, *7*, 10334.

(18) Espinosa, N.; Serrano-Luján, L.; Urbina, A.; Krebs, F. C. *Solar Energy Materials and Solar Cells* **2015**, *137*, 303.

(19) Babagayigit, A.; Thanh, D. D.; Ethirajan, A.; Manca, J.; Muller, M.; Boyen, H.-G.; Conings, B. *Sci. Rep.* **2016**, *6*, 18721.

(20) Stoumpos, C. C.; Malliakas, C. D.; Kanatzidis, M. G. *Inorg. Chem.* **2013**, *52*, 9019.

(21) Baikie, T.; Fang, Y.; Kadro, J. M.; Schreyer, M.; Wei, F.; Mhaisalkar, S. G.; Grätzel, M.; White, T. J. *J. Chem. Mater. A* **2013**, *1*, 5628.

(22) Hao, F.; Stoumpos, C. C.; Cao, D. H.; Chang, R. P. H.; Kanatzidis, M. G. *Nature Photonics* **2014**, *8*, 489.

(23) Noel, N.; Stranks, S. D.; Abate, A.; Wehrenfennig, C.; Guarnera, S.; Haghighirad, A.-A.; Sadhanala, A.; Eperon, G. E.; Pathak, S. K.; Johnston, M. B.; Petrozza, A.; Herz, L. M.; Snaith, H. J. *Energ. Environ. Sci* **2014**, *7*, 3061.

(24) Filip, M. R.; Giustino, F. *J. Phys. Chem. C* **2016**, *120*, 166–173.

(25) Nechache, R. N.; Harnagea, C.; Li, S.; Cardenas, L.; Huang, W.; Chakrabartty, J.; Rosei, F. *Nature Photon.* **2015**, *9*, 61–67.

(26) Berger, R. F.; Neaton, J. B. *Phys. Rev. B* **2012**, *86*, 165211.

(27) van Loef, E. V. D.; Dorenbos, P.; van Eijk, C. W. E.; Krämer, K. W.; Güdel, H. U. *J. Phys.: Condens. Matter.* **2002**, *14*, 8481–8496.

(28) Shannon, R. D. *Acta. Cryst. A* **1976**, *32*, 751–767.

(29) He, Y.; Galli, G. *Chem. Mater.* **2014**, *26*, 5394.

(30) Filip, M. R.; Verdi, C.; Giustino, F. *J. Phys. Chem. C* **2015**, *119*, 25209–25219.

(31) Filip, M. R.; Eperon, G.; Snaith, H. J.; Giustino, F. *Nature Commun.* **2014**, *5*, 5757.

(32) Morrs, L. R.; Robinson, W. R. *Acta Cryst. B* **1972**, *28*, 653–654.

(33) Even, J.; Pedesseau, L.; Jancu, J.-M.; Katan, C. *J. Phys. Chem. Lett.* **2013**, *4*, 2999.

(34) Filip, M. R.; Giustino, F. *Phys. Rev. B* **2014**, *90*, 245145.

(35) Hedin, L. *Phys. Rev.* **1965**, *139*, A796.

(36) Hybertsen, M. S.; Louie, S. G. *Phys. Rev. B* **1986**, *34*, 5390.

(37) Momma, K.; Izumi, F. *J. Appl. Cryst.* **2008**, *41*, 653.

(38) Slavney, A. H.; Hu, T.; Lindenberg, A. M.; Karunadasa, H. I. *J. Am. Chem. Soc.* **2016**, *138*, 2138–2141.

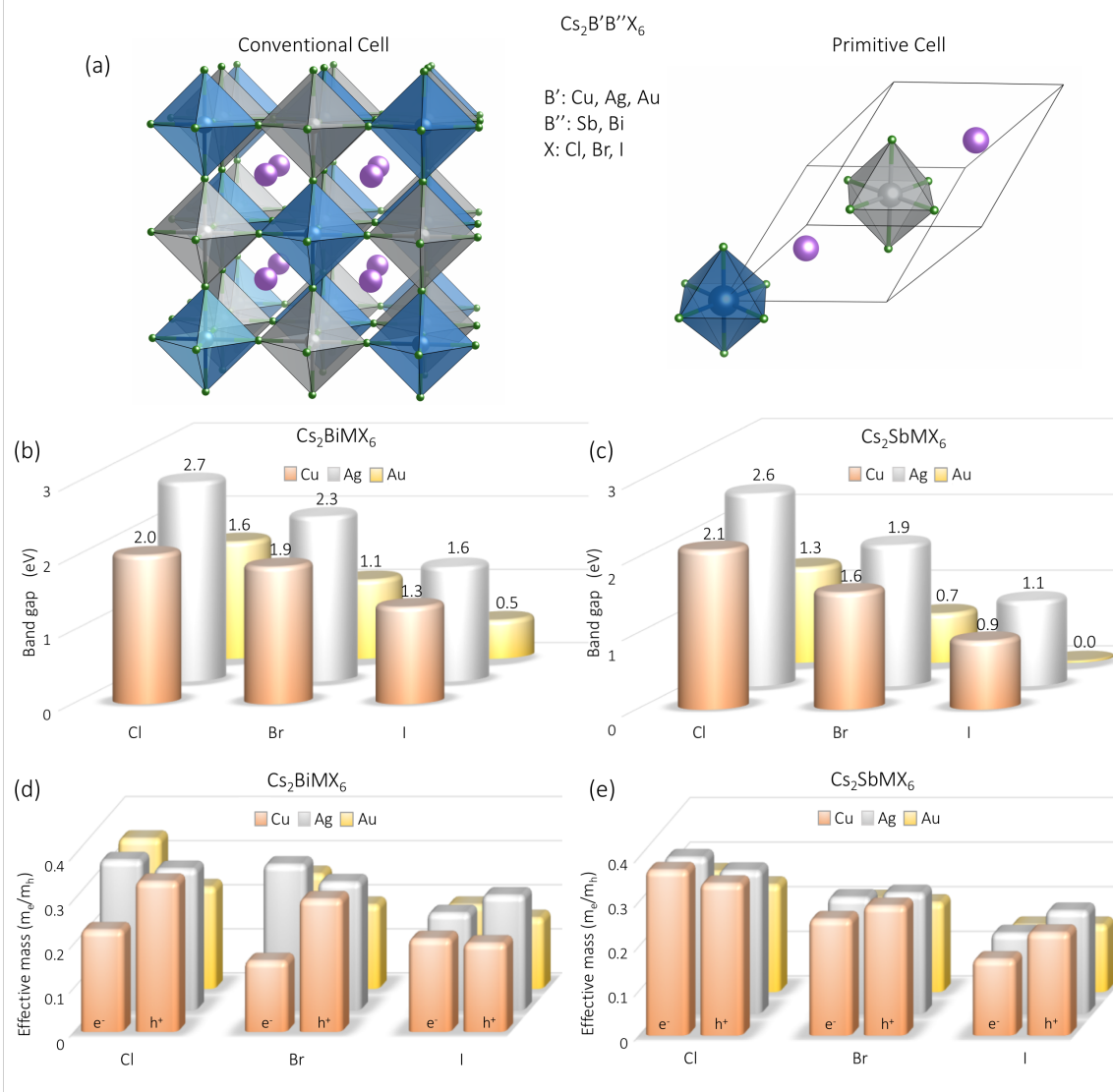(39) McClure, E. T.; Ball, M. R.; Windl, W.; Woodward, P. M. *Chem. Mater.* **2016**, *28*, 1348–1354.

Figure 1: **Computational screening of the electronic properties of the pnictogen-noble metal halide double perovskites**

a Polyhedral model of the conventional (left) and reduced (right) unit cell of the hypothetical halide double perovskites. The pnictogen (B′) and noble metal (B″) cations alternate along the three crystallographic axes, forming the rock-salt ordering. **b** Electronic band gaps calculated for all compounds in the halide double perovskite family using the PBE0 hybrid functionals. All calculated band gaps are indirect with the top of the valence band at the X point $(0,0,2\pi/a)$ of the Brillouin zone, where a is the lattice parameter of the FCC unit cell. The bottom of the conduction band is at the L point $(\pi/a, \pi/a, \pi/a)$ of the Brillouin zone in all cases, except $Cs_2BiAgCl_6$, $Cs_2BiCuCl_6$ and $Cs_2BiCuBr_6$ where the bottom of the conduction band is found at the Γ $(0,0,0)$ point. **c** Conductivity effective masses calculated from DFT/LDA for each compound (see Supporting Information). The effective masses are calculated at the VBM (holes) and CBM (electrons) in each case.
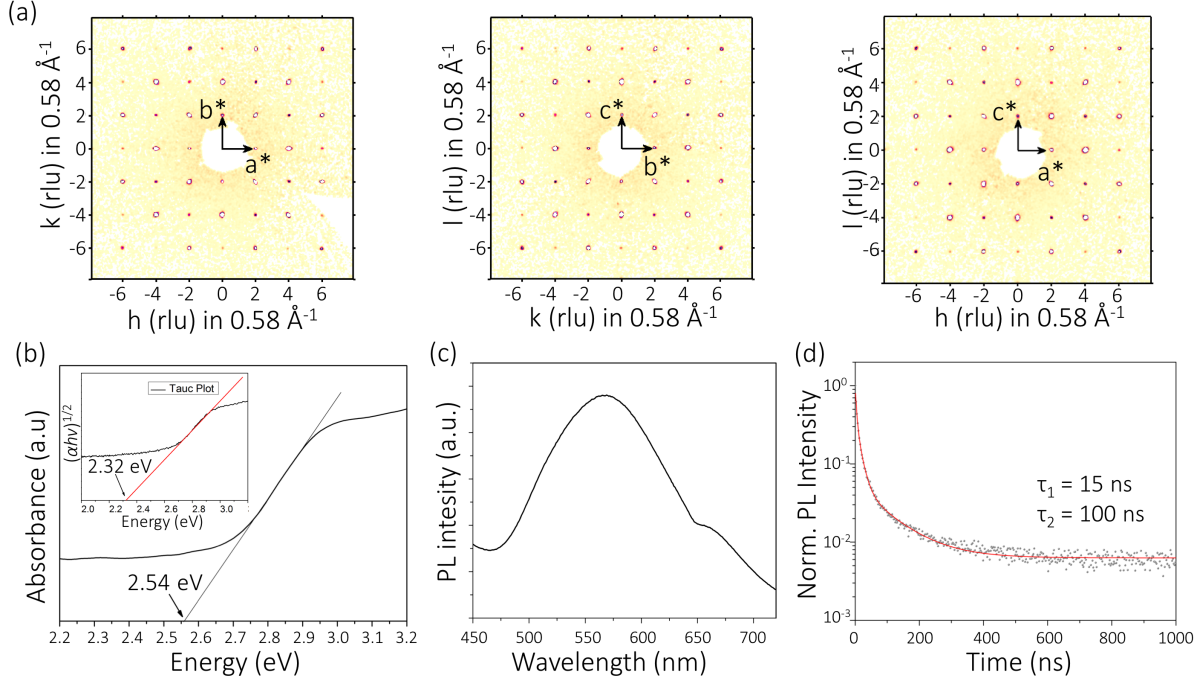
Figure 2: **Experimental synthesis and characterization of $Cs_2BiAgCl_6$.**
a X-ray diffraction pattern for a $Cs_2BiAgCl_6$ single crystal at 293 K. *hkl* shown for three different planes, i.e. $0kl$, $h0l$ and $hk0$. All wave vectors are labeled in reciprocal lattice units (rlu) and a*, b* and c* denote reciprocal lattice vectors of the cubic cell of the $Fm\bar{3}m$ structure. **b** UV-Vis optical absorption spectrum of $Cs_2BiAgCl_6$. The inset shows the Tauc plot, corresponding to an indirect allowed transition [assuming the expression: $(\alpha h\nu)^{1/2} = C(h\nu - E_g)$, where α is the absorption coefficient, $h\nu$ is the energy of the incoming photon E_g is the optical band gap and C is a constant]. The straight lines are fitted to the linear regions of the absorption spectrum and Tauc plot, and the intercepts at 2.32 eV and 2.54 eV marked on the plot are calculated from the fit. **c** Steady-state photoluminescence (PL) spectrum of $Cs_2BiAgCl_6$, deposited on glass. **d** Time resolved photoluminescence decay of $Cs_2BiAgCl_6$, deposited on glass. The data is fitted using a biexponential decay function. The decay lifetimes of 15 ns (fast) and 100 ns (slow) is estimated from the fit.
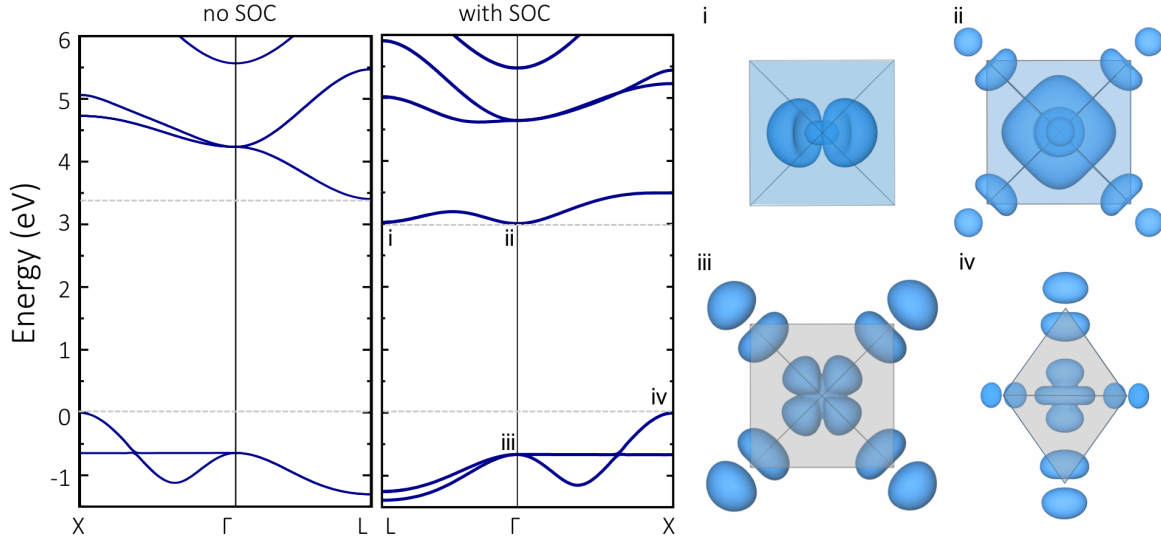
Figure 3: **Electronic structure properties calculated for the experimental crystal structure of $Cs_2BiAgCl_6$.**
The Band structure of $Cs_2BiAgCl_6$ calculated along the high symmetry path $L(\pi/a, \pi/a, \pi/a)$ - Γ (0,0,0) - X (0,0,2π/a) without (left) and with (right) spin-orbit coupling. The black points on the fully relativistic band structure marked 'i-iv' mark the conduction band bottom at L and Γ and the valence band top at Γ and X, respectively. For each of the states we show the electronic wavefunctions. The conduction band bottom is primarily of Bi-p and Cl-p character, while the valence band top consists of Ag-d and Cl-p character. The shape of all four wavefunctions is consistent with metal-halide σ-bonds.